HHS Public Access

Author manuscript

Acta Biomater. Author manuscript; available in PMC 2021 September 01.

Published in final edited form as:

Acta Biomater. 2020 September 01; 113: 164–176. doi:10.1016/j.actbio.2020.06.011.

Highly Tunable Bioactive Fiber-Reinforced Hydrogel for Guided Bone Regeneration

Nileshkumar Dubey[a], **Jessica A. Ferreira**[a], **Arwa Daghrery**[a], **Zeynep Aytac**[a], **Jos Malda**[b,c,d], **Sarit B. Bhaduri**[e,f], **Marco C. Bottino**[a,*]

[a]Department of Cariology, Restorative Sciences and Endodontics, School of Dentistry, University of Michigan, Ann Arbor, Michigan, United States. [b]Regenerative Medicine Center, University Medical Center Utrecht, Utrecht, The Netherlands. [c]Department of Orthopedics, University Medical Center Utrecht, Utrecht, The Netherlands. [d]Department of Clinical Sciences, Faculty of Veterinary Medicine, Utrecht University, Utrecht, The Netherlands. [e]Department of Mechanical, Industrial and Manufacturing Engineering, University of Toledo, Toledo, Ohio, USA. [f]EEC Division, Directorate of Engineering, The National Science Foundation, Alexandria, Virginia, USA.

Abstract

One of the most damaging pathologies that affects the health of both soft and hard tissues around the tooth is periodontitis. Clinically, periodontal tissue destruction has been managed by an integrated approach involving elimination of injured tissues followed by regenerative strategies with bone substitutes and/or barrier membranes. Regrettably, a barrier membrane with predictable mechanical integrity and multifunctional therapeutic features has yet to be established. Herein, we report a fiber-reinforced hydrogel with unprecedented tunability in terms of mechanical competence and therapeutic features by integration of highly porous poly(ε-caprolactone) fibrous mesh(es) with well-controlled 3D architecture into bioactive amorphous magnesium phosphate-laden gelatin methacryloyl hydrogels. The presence of amorphous magnesium phosphate and PCL mesh in the hydrogel can control the mechanical properties and improve the osteogenic ability, opening a tremendous opportunity in guided bone regeneration (GBR). Results demonstrate that the presence of PCL meshes fabricated via melt electrowriting can delay hydrogel degradation preventing soft tissue invasion and providing the mechanical barrier to allow time for slower migrating progenitor cells to participate in bone regeneration due to their ability to differentiate into bone-forming cells. Altogether, our approach offers a platform technology for the development of the next-generation of GBR membranes with tunable mechanical and therapeutic properties to amplify bone regeneration in compromised sites.

Graphical abstract

[*]**Corresponding author:** mbottino@umich.edu (M.C. Bottino).

Declaration of Competing Interest

The authors declare no competing financial interest or with respect to the authorship and/or publication of this article.

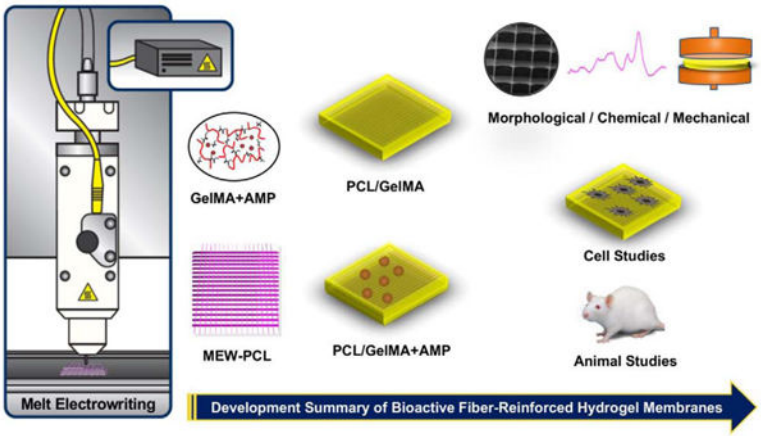

Keywords

Periodontal regeneration; bioprinting; melt electrowriting; magnesium phosphate; hydrogel

1. Introduction

One of the most damaging pathologies that affects the health of both soft (gingiva and periodontal ligament) and hard tissues (alveolar bone and cementum) around the tooth is periodontitis. It is one of the world's most prevalent chronic inflammatory diseases [1, 2]. Considering that approximately 47% of American adults are affected by periodontitis, it is a more prevalent condition than cancer and cardiopathy [1, 2]. Loss of alveolar bone results from the accumulation of a consortium of pathogens including but not limited to *Porphyromonas gingivalis* and activation of inflammatory bone responses, which ultimately may lead to tooth loss [3]. While autografts are considered the standard of care for repairing large periodontal bone defects, their usage is limited due to donor scarcity and site morbidity. Allografts, on the other hand, can impose immunogenic responses due to host-foreign tissue interactions and they can act as a potential for disease transmission [4].

Over the past decades, periodontal destruction has been managed mostly by an integrated approach involving clinical flap debridement/curettage and regenerative strategies [3]. Notably, current treatment modalities to address severe periodontal destruction often result in some form of periodontal tissue repair. Ideally the aspiration should be the complete and certain restoration of architecture and function, *i.e.*, *de novo* formation of gingiva, alveolar bone, a functionally oriented periodontal ligament (PDL), and cementum [3]. Thus, rooted in the principles of tissue exclusion, the application of a physical membrane barrier, either non-resorbable or resorbable serves two purposes: (i) to hinder fast proliferating epithelial tissue from invading the periodontal defect, and (ii) to allow time for slower migrating progenitor cells to recolonize the root area and differentiate into new periodontal tissues. The aforementioned aspects, associated or not with the use of bone grafts and/or exogenous growth factors, have contributed to the advancement of periodontal regeneration [3].

Several authors have discussed the optimal features of membranes for guided tissue regeneration (GTR), or guided bone (GBR) regeneration. These membranes should provide cell occlusion and space maintenance, be biocompatible, and present good handling properties. Of note, many of the current GTR/GBR membranes are composed of polymers, which may be non-resorbable (*e.g.,* polytetrafluoroethylene, PTFE) or resorbable both synthetic (*e.g.,* poly(ε-caprolactone), PCL) or naturally derived (*e.g.,* collagen). Resorbable membranes; however, are preferred as there is no need to perform secondary surgery for membrane's removal, which implicates not only additional discomfort but also an economic burden. Notwithstanding, intrinsic disadvantages related to resorbable membranes including but not limited to relatively fast degradation, shrinkage and collapse of the membrane into the defect [3]. These issues strongly highlight the unmet clinical need in devising a membrane with optimal mechanical strength, degradation rate, and distinctive therapeutic features such as antimicrobial, osteoinductive and regenerative (growth factors and cytokines) properties [3].

In recent years, solution electrospinning – a nanostructured textile-based technique, has been exploited to create polymeric membranes mimicking not only the microstructural aspects of the extracellular matrix (ECM) of native tissues (*e.g.,* fiber diameter and pore size), but also the physicochemical properties key in tissue regeneration [3]. Moreover, electrospun nanofibers can be loaded with biomolecules and/or compounds that provide multifunctionalities (*e.g.,* antimicrobial, anti-inflammatory, and cell differentiation abilities) in the quest to engineer membranes with much needed therapeutic attributes [3]. However, inherent difficulties associated with the distribution of controlling pore size and more importantly to engineer defect-specific membranes to amplify both hard and soft periodontal tissue regeneration have limited its clinical translation [5]. The aforesaid limitations associated with solution electrospinning have led to the consideration of additive manufacturing (AM) techniques, such as fused deposition modeling to design membranes with increased porosity and three-dimensional (3D) architecture [6].

Hydrogels offer great versatility in design and synthesis and have attracted great attention for GBR due to the ease of encapsulating therapeutics and/or cells [7–9]. They have inherent biocompatibility, biodegradability, and possess biologically recognizable moieties that support cell adhesion/proliferation through a fully hydrated 3D microenvironment [3]. Moreover, the physicochemical and biological properties of hydrogels can be further tuned to closely match the properties of their targeted tissues of interest [3]. Nonetheless, often times hydrogels present suboptimal biomechanics, which in turn do not provide a favorable environment to encapsulated cells or make them too weak for applications in periodontal tissue engineering. This is even more so, when designed to function as a physical barrier in GTR/GBR applications. Therefore, three major approaches, namely (i) incorporating micron-sized and/or nanosized inorganic particles, (ii) increasing the hydrogel polymer concentration or crosslink density, and (iii) incorporating nano- or microfibers to enhance biomechanical properties have been used. For example, a versatile composite system consisting of highly porous PCL fibrous meshes with well-controlled 3D architecture processed via melt electrowriting (MEW) and a gelatin-methacryloyl (GelMA) hydrogel was able to synergistically enhance the mechanical strength, while displaying outstanding biological performance [10–12]. Meanwhile, the strategy of encapsulating bioactive

materials, such as tricalcium phosphate particles, to amplify hydrogels' stiffness has also garnered considerable interest [7, 8]. Of note, unique to the present investigation, unlike calcium phosphates (CaP), recently synthesized amorphous magnesium phosphate (AMP) has shown a higher proliferation rate and osteogenic gene expression compared to its CaP counterparts [13–15].

Altogether, inspired by these remarkable findings, the aim of this work was to engineer, by perfusing a MEW PCL mesh with an AMP-laden hydrogel, highly tunable bioactive fiber-reinforced membranes for GBR. GelMA is a photopolymerizable hydrogel that can be cured by visible dental light-curing devices [16]. Moreover, GelMA can maintain a moist environment at the bone defect interface, allowing for gaseous and fluid exchange, removing excess exudates, and supporting cell infiltration and integration [17]. Therefore, we postulated that the integration of highly porous PCL fibrous mesh with well-controlled 3D architecture into a AMP-laden hydrogel can control the mechanical behavior and improve the osteogenic properties of GelMA opening an opportunity to be used as a bioactive GBR membrane. The effects of infusing PCL with a bioactive AMP-laden hydrogel, as well as the extent of *in vitro* and *in vivo* osteogenesis, were comprehensively examined. We demonstrate that the presence of PCL meshes fabricated via MEW can delay hydrogel degradation preventing soft tissue invasion and providing the mechanical support for recruitment and differentiation of progenitor cells to prompt bone tissue regeneration. The current approach of reinforcing AMP-laden hydrogels with MEW PCL meshes offers a platform technology that can be further leveraged in the design of next-generation GBR membranes with unique bioactive features and tunable mechanical properties to amplify tissue regeneration in compromised bone sites.

2. Materials and Methods

2.1. Materials and chemicals

Poly(ε-caprolactone) (PCL, Mn:5000, CELLINK, Gothenburg, Sweden), sodium hydroxide (NaOH, Sigma-Aldrich, St. Louis, MO, USA), ethanol (99.5%, Sigma-Aldrich) were purchased and used as received without any further purification. Distilled-deionized (DI) water from a Millipore Milli-Q ultrapure water system was used in the experiments. Magnesium nitrate hexahydrate and diammonium hydrogen phosphate were procured from Sigma-Aldrich.

2.2. Melt electrowriting (MEW)

PCL is an FDA approved polymer widely used for periodontal regeneration due to favorable biocompatibility and the ability to be processed into various design including membranes via 3D printing technologies [3, 18]. Here, PCL meshes were fabricated via melt electrowriting (MEW) using a highly translational multi-head bioprinting platform (3DDiscovery, regenHU, Villaz-St-Pierre, Switzerland) in a biosafety cabinet. The system moves on the x, y, and z axes with a printhead moving in the x and z direction and the collector platform moving in the y-direction. The MEW printhead has a high voltage power supply, an electrical heating system to control the temperature, and a pneumatically regulated feeding system. Printing path designs were created using BioCAD; a G-code file was obtained, then

loaded to HMI software for printing. Briefly, in order to produce polycaprolactone (PCL) meshes, PCL pellets were placed in a metal cartridge having 26 G of the nozzle and the cartridge was heated to 90°C for 30 min to allow enough time for the polymer to melt. The system's pressure was adjusted to 0.07 MPa. The PCL mesh was printed using a feed rate of 40 mm/s and −7 kV of voltage was applied from a distance of 4 mm. The 0/90°crosshatch design, having 500 μm of space, was printed on top of each other to form a PCL mesh with 450 layers. The MEW PCL mesh was etched to increase hydrophilicity [12]. First, the meshes were soaked in 70% ethanol for 15 min, and then they were immersed in a 5 M of sodium hydroxide (NaOH) aqueous solution for 4 h at room temperature (RT). After etching, the meshes were washed with DI water until neutral pH was reached. Finally, they were air-dried overnight.

2.3. Gelatin methacryloyl (GelMA) synthesis and preparation of AMP-laden GelMA

GelMA was synthesized as described previously [19]. Briefly, 10% (w/v) gelatin (Type A,300 bloom from porcine skin, Sigma-Aldrich)) was dissolved in DPBS at 50°C, followed by methylacrylation with methacrylic anhydride (Sigma-Aldrich) at a rate of 0.5mL/min for 1 hr. The reaction was stopped by diluting with 5× of warm DPBS, and the resulting solution was dialyzed against deionized water through dialysis tubing (12–14 kDa molecular weight, Sigma-Aldrich) for 7 days at 40°C to remove low molecular-weight impurities. The dialyzed solution was lyophilized for 7 days to generate white porous foam. 20% GelMA hydrogel was obtained by dissolving porous foam in DPBS. AMP synthesis was carried out in-house, based on the ethanol-assisted precipitation method. Briefly, 11.5 g of magnesium nitrate hexahydrate ($Mg(NO_3)_2.6H_2O$, Alfa Aesar, 98% purity) was added to 100 ml of water and 100 ml of ethanol and mixed properly. This solution was then rapidly added at 37°C under constant stirring to a solution containing 2.9 g of diammonium hydrogen phosphate ($(NH4)_2HPO_4$, Fischer, 99% purity) in 250 ml water, 45 ml ammonia (11 M), and 295 ml ethanol. A precipitate that formed immediately was collected, centrifuged, and washed in ethanol. Next, 2.5% and 5% AMP (% w/v) was incorporated into the GelMA and left under vigorous stirring at 50◦C for 1 h until a homogeneous dispersion of the AMP was achieved. Crosslinking the fabricated hydrogel was achieved by 0.05% (w/v) lithium acylphosphonate photoinitiator (LAP, Sigma-Aldrich) and photocrosslinked using a LED light-curing device (Bluephase, Ivoclar-Vivadent, Amherst, NY, USA).

2.4. Membrane preparation

MEW PCL meshes were placed in 70% ethanol for 15 min, followed by washing (3×) with DI water. The samples were etched with 5 M NaOH at RT for 4 h in a shaker. The PCL meshes were then washed (5×) with DI water until a neutral pH was reached. For the preparation of the fiber-reinforced membranes (GelMA/PCL), PCL mesh was placed in custom-made (8×8×2 mm) silicone molds (Henry Schein, Inc., Melville, NY, USA); they were then perfused either with GelMA or AMP-laden GelMA. The molds were tapped to ensure complete coverage of the PCL mesh and good hydrogel infiltration into the porous meshes. Finally, hydrogel photocrosslinking was performed with LAP using visible light for 60 s. The prepared membrane groups were named: GelMA (G), GelMA+PCL (GP), GelMA +2.5%AMP (GA2.5%), GelMA+5%AMP (GA5%), GelMA+PCL+2.5%AMP (GPA2.5%) and GPA5% (GPA5%).

2.5. Morphological, chemical, and biomechanical characterizations

Fourier-transform infrared spectroscopy (FTIR) was used to characterize the presence of specific chemical groups in GelMA and MEW printed meshes to study the interactions between the incorporated AMP in GelMA. 16 scans with spectra between 4000 and 500 cm $^{-1}$ at 4 cm^{-1} resolutions were used for both references and samples using the Attenuated Total Reflectance-Fourier transform infrared spectrometer (ATR-FTIR, Thermo-Nicolet iS-50, Thermo Fisher Scientific Inc., Waltham, MA, USA). Baseline correction spectra were then centered and normalized for analysis.

Stereomicroscopy (Zeiss Stemi 508, Carl Zeiss Meditec AG, Oberkochen, Germany) in bright-field mode was used to investigate the morphology of the engineered GelMA/PCL membranes. The morphological assessment of the PCL meshes was carried out by scanning electron microscopy (SEM, MIRA3, FEG-SEM, TESCAN). Printed meshes were mounted on Al stubs by using double-sided carbon tape and sputter-coated (SPI-Module Carbon/ Sputter coater, Thermo Fisher Scientific Inc.) prior to SEM imaging. For some SEM images taken, the stage was tilted at certain angles from 20°–45°. At least 50 pores from 5 SEM images were used to calculate the porosity of the printed meshes (ImageJ, NIH, Bethesda, MD, USA). Cross-sectional views of the fiber-reinforced membranes were obtained by sectioning to visualize the internal structure.

To evaluate the mechanical properties, cylindrical-shaped membrane samples of different thicknesses (0.5 mm to 2 mm) were processed. Further, the effect of the number of PCL meshes for reinforcement of GelMA was also examined. Samples were incubated in DPBS at 37°C. After 24 h, the samples were dried using low-lint paper and then subjected to unconfined compression at a strain rate of 0.5 mm/min (MTESTQuattro, ADMET Inc., Norwood, MA, USA) at RT. A minimum of 8 samples per group was tested. The compressive modulus (stiffness) was calculated from the engineering stress-strain curves in the linear region corresponding to the 0–20% strain.

Estimation of volumetric hydrogel fraction of fiber-reinforced membrane. Assuming the mold (8-mm base side and 2-mm height) and pore of the MEW mesh were filled with hydrogel (V_m), the theoretical hydrogel content of the fiber-reinforced membrane immediately after the molding process was determined volumetrically using the equation below:

$$\text{Volumetric hydrogel fraction}(\%) = (V_m - V_f)/V_m) \times 100$$

The weight of the printed mesh (n=20) was measured using a microbalance. The volume of the fibrous network (V_f) was calculated as follows: V_f= Mass of printed mesh/Density of PCL [PCL=1.145 g/cm^3].

2.6. Cell culture

Human mesenchymal stem cells derived from bone marrow (hMSCs, Lonza, Basel, Switzerland) at passage 3 were cultured in Mesenchymal Stem Cell Growth Medium

(MSCGM™; Lonza) and incubated in an atmosphere of 95% relative humidity and 5% CO_2 at 37°C. Cells between the third to sixth passages at 70–80% of confluence were used.

2.7. Cytocompatibility and morphology

To confirm the cytocompatibility character of the etched MEW PCL mesh and engineered membranes, 1×10^6 and 2×10^5 MSCs were seeded per sample, respectively and cell proliferation was evaluated using MTS assay (CellTiter 96 AQueous One Solution Assay, Promega Corporation, Madison, WI, USA). At predetermined time points, the cells were incubated for 2 h and absorbance was measured in a microplate reader at 490 nm (Spectra iD3; Molecular Devices, LLC, San Jose, CA, USA). For fluorescence, the cells were fixed with 4% PFA for 30 min at RT, followed by permeabilization with 0.1% Triton X-100 in PB for 5 min at RT. The cells were then washed with PBS and blocked using 1% BSA for 30 min, followed by staining with TRITC-conjugated phalloidin and DAPI (1:1200, Millipore Sigma Company, Burlington, MA, USA) for 1 h according to the manufacturer's instructions; samples were imaged using an upright fluorescence microscope (Carl Zeiss). SEM was done to observe cell morphology at day 5 on the membranes' surface. The cells were fixed with 4% paraformaldehyde for 30 min, followed by washing with PBS (2×) for 5 min each. Samples were imaged using a low vacuum Tescan Rise electron microscope (Tescan USA, Inc., Warrendale, PA, USA).

2.8. Alizarin red staining

The mineralization potential of the engineered membranes was quantitatively and qualitatively assessed using Alizarin red staining (ARS, Sigma-Aldrich). MSC at a density of 1×10^4 per membrane was seeded and the media was replaced with fresh media every 3 days up to 21 days. On days 14 and 21, the cells were washed with PBS (2×) and fixed in 4% formaldehyde at RT for 30 min, followed by another washing with PBS (2×) for 20 min. The cells were then stained with 40 mM ARS and the plates incubated at RT for 30 min, washed with DI water (4×), dried and scanned with the Epson Perfection V50 photo scanner (Epson Inc., Long Beach, CA, USA) and converted into binary images. Thereafter, destaining of the ARS was done using 10% acetic acid and ammonium hydroxide. Finally, the absorbance of the aliquots (100 μL) of the supernatant was measured using a microplate reader (Spectra iD3) at 405 nm.

2.9. Real-time PCR

Osteogenic gene expression of Runt-related transcription factor 2 (RUNX2, Hs01047973_m1), collagen alpha 1 (COL1A1, Hs00164004_m1) and osteopontin (OPN, Hs01587814_g1) were determined by a quantitative polymerase chain reaction (qPCR). Glyceraldehyde 3-phosphate dehydrogenase (GAPDH, Hs02758991_g1) was used as the housekeeping gene. Briefly, the cells were harvested, and the total RNA was isolated (Purelink RNA Mini Kit, Invitrogen, Carlsbad, CA, USA). cDNA synthesis was then performed using iScript RT Supermix (Bio-Rad Laboratories, Inc., Hercules, CA, USA). The ΔΔCq method was used to calculate the relative gene expression from the quantification cycle (Cq) values obtained by RT- PCR. Three independent PCR reactions were performed for each sample.

2.10. In vivo studies

Animal experiments were approved by the University of Michigan Institutional Animal Care and Use Committee (IACUC, protocol #PRO00008502). For the experiments, 6-week-old male Fischer 344 rats (300–320g) were procured (Envigo RMS, Inc., Oxford, MI, USA). All surgical procedures were performed under general anesthesia induced with inhalation isoflurane (Piramal Critical Care Inc., Bethlehem, PA, USA) (4–5%) for induction and maintained with isoflurane (1–3%). For each rat, critical-size bilateral calvarial defects 5-mm in diameter were created using a trephine bur (Trephines 229XL RA; L Size #229XL-050-RAL, 5.0 mm Inside/6.0 mm Outside Diameter, Meisinger USA, LLC, Centennial, CO, USA) (Figure 7). This defect is considered a critical-size bone defect – would not spontaneously heal during the lifetime of the animal [20]. The rats were randomly allocated into Sham (Defect only – Negative Control), G, GP, GA5%, and GPA5%. Square-shaped (6 x 6 mm^2 and 2-mm thick) membrane samples were implanted into the bone defects. After surgery, the animals were subcutaneously medicated with non-steroidal anti-inflammatory drugs (5 mg/kg Carprofen® base, Pfizer, Inc., New York, NY). After 4 and 8 weeks, the animals (n=6/time point) were euthanized by CO_2 and the skulls were collected. The calvaria of the rats were harvested, and the muscle tissue and epiphyses were removed. Subsequently, the bone/membrane was immersed in a 4% paraformaldehyde solution for further analysis.

2.11. Micro-computed tomography (micro-CT)

Non-destructive analysis of the newly formed bone at the bone defect was performed (Scanco μCT 100 Medical AG, Wangen-Brüttisellen, Zurich, Switzerland). Samples were scanned with pieces in 360° rotation using 70 kV, 114 μA monochromatic x-rays, and 25 μm voxel sizes. The exposure time was maintained at an average of 3 frames per 500 ms. The Scanco Medical System software was used for image reconstruction. The reconstructed 3D image was then traced to the circumference of the original defect, which hereafter was referred to as the region of interest (ROI). The ROI of each specimen around the defect was analyzed for tissue volume (TV), bone volume (BV), and bone volume fraction (BVF, BV/TV).

2.12. Histological analysis

After the micro-CT scans, the calvaria samples were decalcified with 10% formic acid solution. The decalcified specimens were dehydrated in an ascending alcohol series, followed by infiltration and embedded with paraffin, then cut into 4-μm sections. The sections were either stained with Hematoxylin and Eosin (H&E) or Masson's trichrome for microscopic examination. The stained sections were observed with a light microscope equipped with a digital camera (Nikon E800, Nikon Corporation, Tokyo, Japan). H&E staining revealed the cellular reaction that indicates bone formation. Masson's trichrome staining was used to identify mineralized bone (blue) and osteoid (red).

2.13. Statistical analysis

All values are expressed as the mean ± standard deviation of 3 independent experiments. The statistical analysis was performed using one-way analysis of variance (ANOVA) followed by Tukey's multiple post-hoc tests (α=0.05).

3. Results and Discussion

3.1. Morphological analysis and cell attachment on MEW PCL mesh

While printing the MEW PCL meshes, the temperature in the cartridge was first determined to completely melt at 60°C; therefore, a temperature of over 60°C was elected. Since increasing the temperature too much might cause instability, it was gradually increased until a stable flow of polymer melt was obtained with the appropriate pressure, which, in our system was 0.07 MPa for PCL melted at 90°C [21, 22]. The second step was to determine the suitable feed rate for the polymer flow and air pressure applied. Here, matching the speed of the jet and collector is of great importance. If the feed rate is lower than the collector, buckling is observed (Fig. 1). Therefore, the feed rate was gradually increased to 40 mm/s until straight and uniform fibers were achieved [21, 22]. Finally, the right combination of electric voltage and distance between the nozzle tip and the collector was decided [21, 22]. As a result, the highest quality of fibers with a uniform structure and the lowest fiber diameter was achieved with the following parameters: temperature: 90°C; air pressure: 0.07 MPa; feed rate: 40 mm/s; high voltage: −7 kV; and distance from nozzle tip to collector: 4 mm (Figure 1). In addition, even though fibers with a smaller diameter or spacing lower than 500 μm were also obtained, it was of vital importance to have a uniform diameter and spacing during the production of the 450 layers used throughout the work.

SEM micrographs of MEW PCL mesh given in Fig. 2 with various tilt angles showed that the fibers are uniform and straight without any defects. SEM micrographs also show that the spacing of the MEW PCL scaffold is 500 μm with well-aligned fibers having an average fiber diameter of 3.2 ± 0.1 μm. In addition, the porosity of the MEW PCL scaffolds was calculated at 91.7 ± 1.6%. It is well-known that scaffolds' architecture, porosity and morphology play a significant role in cell function [23]. Of note, lower cell adhesion and retention on porous PCL has been associated with PCL's intrinsic hydrophobicity [6]. Hence, we investigated the adhesion of bone marrow-derived human mesenchymal stem cells (hMSCs) on NaOH-etched MEW PCL meshes using both fluorescent and scanning electron microscopy (SEM) after 3 days of culture. SEM micrographs (Fig. 2) exhibited favorable growth of hMSCs with flattened morphology and characteristic phenotype that were able to extend their cellular processes into and around the melt-electrowritten PCL fibers mostly at the intersections of fibers of different layers (Fig. 2), which was found not only at intersections, but also along MEW PCL fibers allowing cell interaction between pore structures. This finding is in accordance with previous published literature for PCL etched with NaOH in terms of cells producing filamentous extension with elongated cell morphology [24].

Stereomicroscope analysis was carried out to examine the infusion of GelMA and GelMA +AMP hydrogels into MEW PCL meshes. Fig. 3A confirms the penetration of the hydrogel

phase in the PCL porous mesh leading to the formation of a hybrid fiber-hydrogel membrane. Fig. 3B–E show cross-section SEM micrographs of the fiber-reinforced membranes, further evidencing the uniform infiltration of the hydrogel into the porous PCL meshes. Of note, the presence of the hydrogel phase within the pores of the PCL mesh can also prevent soft tissue penetration into the periodontal defect during the healing phase, thus allowing for timely cell recruitment, proliferation and differentiation. Noteworthy, in the fiber-reinforced membranes, hydrogel is the primary constituent, where the volumetric hydrogel fraction of the membrane was 95.2 ± 0.3%.

3.2. Chemical analysis – Fourier transform infrared spectroscopy (FTIR)

The FTIR spectra (Fig. 3F) of the MEW mesh showed characteristics PCL peaks at 2865 cm $^{-1}$ and 1720 cm^{-1}, corresponding to CH_2 and C=O stretching, respectively [25]. This indicates that melt electrowriting can print fibers without affecting the chemical composition of the polymer. Moreover, the functional groups related to phosphate (~ 1079 cm^{-1}) in GelMA+AMP, along with a typical amide band due to the presence of gelatin in the hydrogel, confirms, as expected, the successful AMP incorporation into GelMA [15, 26].

3.3. Biomechanical properties

The stiffness values of the membranes are shown in Fig. 4A. In general, membranes produced with a 0.5–1.5 mm hydrogel thickness of GP (GelMA+PCL), GA2.5% (GelMA +AMP2.5%), and GPA2.5% (GelMA+PCL+AMP2.5%) showed significantly greater stiffness than GelMA (G), except 5%AMP membranes (GA5% and GPA5%). Of note, although it is clear that the presence of a single PCL mesh within 0.5–1.5-mm thick hydrogel membranes led to a significant increase in stiffness, the addition of AMP (2.5 and 5%) reduced the stiffness values compared to GP. Previous studies have shown that bioceramics inclusion into hydrogel can lead to enhanced mechanical properties [17, 27, 28]. Nonetheless, the limited dispersibility of bioceramic particles can lead to agglomeration, which acts as structured defects leading to reduced stiffness, as observed in our data. Importantly, 2-mm thick membranes showed nearly similar stiffness compared to GelMA (G), irrespective of the AMP content or PCL mesh presence. Furthermore, although the reduction in stiffness for AMP-modified (2.5 and 5%) membrane formulations could be attributed to incomplete crosslinking of GelMA+AMP, as the addition of AMP into the GelMA makes the hydrogel opaque [29, 30], the stiffness data did not support that assumption. Notably, since there were no significant differences among the groups tested compared to un-modified GelMA (G), it is difficult to categorically infer that the opacity of the resultant membrane was the sole factor responsible for the observed difference between G and GPA5%. Hence, this aspect should be systematically explored in future studies; for example, by monitoring crosslinking kinetics of AMP-modified GelMA using in-situ polymerization in a time-sweep oscillatory test.

Most studies aimed at the mechanical reinforcement of hydrogels with a MEW polymer mesh resulting in increased stiffness of 10- to 50-fold compared to the hydrogel alone [12, 31, 32]. In our study, 2-mm thick GelMA incorporated with a single PCL mesh showed stiffness similar to the hydrogel. In order to further explore the underlying mechanism causing the fiber-reinforcement effect, we investigated the mechanical behavior of GelMA

infusion through 4 PCL meshes (Fig. 4B–C). The infused fiber in the hydrogel prevent the outflow of the water from the hydrogel is one of the key mechanisms in the enhancement of the mechanical properties of the reinforced hydrogel [12]. As shown in Fig. 4B, the PCL mesh present ca. in the center of the hydrogel might not be able to prevent the horizontal expansion of the hydrogel during unconfined compression and a slower strain rate might provide enough time for water to outflow, therefore, leading to lower stiffness [31]. Nevertheless, 4-PCL meshes infused with GelMA under compression will transform the axial forces into lateral forces, which are carried by the fibers of the meshes leading to high compressive modulus. Moreover, mechanical reinforcement decreases when membrane thickness increase, can be likely due to a higher volume of hydrogel fraction, which decreases the surface area available for the hydrogel to bind with the polymeric network [31]. In aggregate, highly tunable hydrogel can be obtained by two ways – by varying the amount of AMP into the hydrogel and by increasing the number PCL meshes.

3.4. Cytocompatibility – cell attachment and proliferation

Cytocompatibility of membranes for GBR is one of the most important characteristics for tissue regeneration [3]. Indeed, an ideal membrane should have cell affinity and tissue adhesiveness to achieve successful periodontal reconstruction. Representative fluorescence and SEM micrographs (Fig. 5) show that hMSCs displayed typical fibroblast-like appearance and were able to attach and proliferate on the engineered membranes. Likewise, we investigated cell proliferation (MTS assay) on the different membranes fabricated with and without AMP and/or PCL mesh (Fig. 6A). All the groups showed higher cell proliferation compared to GelMA alone at all time points. The increased proliferation rate was dependent on the presence of AMP and its content (2.5% vs. 5%), where the GPA5% membrane showed the highest proliferation. Prior to the 3rd day, the proliferation rate between membranes with dissimilar AMP amounts was not significant; however, on the 5th day, there was a significant difference between GA2.5% and GA5% membranes, and the presence of PCL further increased the proliferation rate. Our data agree with previous literature regarding MEW PCL-reinforcement of hydrogels [12, 32] and incorporation of β-TCP in GelMA where proliferation of hASCs was 127% on day 1, as compared to GelMA, and implants coated with AMP showed increased viability due to the stimulatory effect of the apatite [7, 33]. Notably, the developed membrane and GelMA presented dimensional stability and integrity throughout the *in vitro* culture suggesting that the stiffness of the developed membrane was suitable for cell proliferation and migration. Nonetheless, MEW PCL meshes allowed cell attachment displaying biomimetic microenvironment for cell growth and distribution. Altogether, we postulate that the gradual degradation of GelMA and good cell attachment ability of the PCL mesh could facilitate cell infiltration, nutrition, and tissue formation (Fig. 2).

3.5. Mineralization and osteogenic gene expression

Another key aspect of next-generation GBR membranes is that they should possess chemical functionality to amplify the mineralization and osteogenic differentiation of resident cells upon implantation. Hence, after confirming the cytocompatible character of the engineered membranes (Fig. 6A), we assessed their ability to promote osteogenic differentiation *in vitro*. After 14 and 21 days of culture, mineralization of the extracellular matrix, assessed by

Alizarin assay presented the characteristic red staining representing mineralization (Fig. 6B). Calcium deposits increased with AMP concentration in a time-dependent manner. Further, the integration of PCL into the hydrogel showed significant effect on mineralization. This indicates that rigid support of porous hybrid scaffolds has improved mineralization of the bone matrix. This was further demonstrated through the expression of osteogenic genes RUNX2, COL 1, and OPN (Figure 6C–D). RUNX2 (core-binding factor alpha-1 Cbfa1) is a member of the runt homology domain family of transcription factors involved in the upregulation of specific ECM protein related to bone formation, such as osteopontin (OPN). In the results of GPA5% at 14 days, RUNX2 and OPN were expressed 4 times and 3.5 times more than GelMA, respectively (Fig. 6C). This can be due to the hydrolysis of the AMP resulting in Mg^{2+} and HPO_4^{2-} release, which, in turn, enhances osteogenic differentiation [15, 34]. Hence, the integrated membrane with AMP promoted higher matrix mineralization as compared to the other membranes. Interestingly, there was no significant difference between the COL 1 expression among the GPA2.5%, GPA5%, and GA5% membranes. Accordingly, at 21 days, PCL mesh infused with GelMA+AMP expressed higher levels of RUNX2 and OCN compared to GelMA+AMP (i.e., GA2.5% and GA5%) membranes (Fig. 6D). A similar increase had been observed when stem cells were seeded or encapsulated in poly(L-lactide-co-ε-caprolactone) (P(LLA-CL)) nano yarns suspended in type I collagen hydrogel [35] or 3D printed PCL scaffolds integrated with hydrogel [6, 12]. It has been noted that the presence of AMP activates osteogenic genes during cell proliferation and differentiation that closely matches the expression levels achieved with CaPs [15]. Similar results were reported by previous studies involving AMP, demonstrating expression levels of all the osteogenic markers increased with time and AMP content [13, 33, 34, 36]. Overall, the PCL mesh infused with bioactive hydrogel facilitated the osteogenic differentiation and mineralization of MSCs as compared to the PCL mesh infused with pristine (blank) GelMA.

3.6. In vivo bone regeneration

Bone defect regeneration remains a critical challenge and require bone grafts or bone substitutes with the ability to control cell fuction, osteoinductive properties, and biodegradability [1]. To understand the general clinical prospect of the fiber-reinforced hydrogel membranes, herein we used a well-established bilateral critical-size calvarial defect in rats (Fig. 7). Over the past decades, the rat calvarial defect has been utilized to study bone regeneration and screen distinct biomaterials/scaffolds prior to implantation in larger animals for potential human translation [37]. Of note, the calvarial defect model shares anatomical similarities with the human mandible (*i.e.*, two cortical plates with intervening cancellous bone) and the developmental pathway of bone formation [38–40]. Further, the model mimics the clinical scenario of a 3-wall periodontal defect, which allows bone formation from the bottom and circumferential walls of the defect. Importantly, similar to what happens in periodontal defects, the rat calvarial defect will be filled with fibrous connective tissue, if space maintenance in the form of a membrane is not provided [41]. In the present study, new bone formation was observed from the margin of the defect site in for all groups after four weeks of implantation. However, even after 8 weeks of implantation, the negative control (Sham group) and GelMA membrane showed minimal bone formation, while bone formation was more obvious in the presence of AMP and PCL (Fig. 8A). This can be explained through the enhanced and accelerated mineralization of AMP added into

GelMA infused PCL [33, 36]. Besides the qualitative results provide by micro-CT 3D reconstruction, bone formation was further confirmed with quantitative outcomes (Fig. 8B). The results indicate that the amount of bone volume (BV) in the defects displayed that the newly formed bone tissue was almost 6-fold in GA5% group compared to sham after 8 weeks indicating that the enhancement of *in vitro* osteogenic efficacy by AMP was also effective *in vivo.* The infusion of PCL mesh with GelMA+AMP hydrogel further enhanced the volume of new bone formation by 8-fold, which may be correlated with the additional inductive effect of highly ordered micron-sized fibers [35, 42]. The micro-CT data were further supported by histological analysis based on H&E and Masson's trichrome staining of decalcified bone (Fig. 9). After 4 weeks, the defect area in the negative control (defect-only) was filled with fibrous connective tissue and only a small amount of bone was formed near the edges (Fig. 9). The early phase of new bone formation was observed at the margin of the calvarial defect in the GelMA hydrogel and experimental groups. In the GelMA group, there were more inflammatory cells and collagen. In the GP, GA5% and GPA5% groups, newly formed bone was well-integrated from the original edges of the bone defect. Masson' trichrome staining showed tight distribution of regenerated collagen tissues in defect sites implanted with GelMA+AMP infused PCL membranes (Fig. 9). Rats in the GA5% and GPA5% showed mature new bone formation that was completely integrated with host bone tissue at the defect edge. As previously mentioned, the ability to prevent the invasion of soft tissue into the periodontal defect and allowing time for resident cells to initiate neo-tissue formation is key for successful GBR therapy [3]. Therefore, although previous studies have supported the contribution of stem cell transplantation to enhance bone formation, it is clinically pertinent to state that cell-based approaches not only pose regulatory obstacles but also potential threats of host immune responses and uncontrolled cell differentiation [43]. Hence, the aim of this investigation was to engineer a bioactive (AMP) fiber-reinforced hydrogel membrane as a cell- and growth factor-free strategy for guided bone regeneration. This work sought the addition of PCL and AMP will maintain membrane shape and volume longer in contact with tissue, improving the recruitment of osteogenic cells into defect which can be favorable in achieving the required width and vertical bone height during periodontal/bone regeneration. As seen in Fig. 9, small pieces of GelMA hydrogel was present in the groups treated with GA5% and GPA5% membranes, even 8 weeks post-implantation, indicating slower degradation of GelMA when PCL and AMP were added, signifying superior barrier function of the engineered fiber-reinforced bioactive membrane. A similar study was conducted using 5-mm rat calvarial defect model covered by GelMA and GelMA with beta tri-calcium phosphate (β-TCP) showed new bone as scattered and island-like structures after 8 weeks, which might be due to the penetration of soft tissue across the scaffold leading to incomplete bridging of the defect. Moreover, microCT demonstrated β-TCP was not completely degraded [7]. Further, according to our data, one might expect that both membrane thickness and stiffness can influence space-maintaining properties upon membrane implantation. Previous research has shown that thicker membranes allow less soft tissue ingrowth and better bone formation [44]. In light of our positive findings and the opportunities to tune the biomechanical properties of the proposed bioactive fiber-reinforced hydrogel membranes, further research, including but not limited to studying the impact of thickness on membrane degradation and osteogenesis, need to be investigated. Nevertheless, our results highlight the advantage of the presence of a microfibrous structure to prevent soft

tissue invasion and rapid hydrogel degradation to enhance the bone regeneration. Taken together, GPA5% offers advantages where prolonged membrane barrier functions are desirable. The integration of PCL fibrous mesh in bioactive AMP-modified hydrogel positively affects bone regeneration (Fig. 10), and thus lays the groundwork for the next phase of this endeavor, which will involve the use of a large animal model of vertical bone augmentation such as a canine mandibular model.

4. Conclusions

This work represents a major step towards developing highly tunable fiber-reinforced bioactive membranes by combining melt electrowritten (MEW) high-porosity PCL meshes with hydrogels doped with ceramic particles with intrinsic bioactivity, such as amorphous magnesium phosphate (AMP). The stiffness of the engineered membrane was significantly enhanced, and this reinforcing effect can be modulated by altering the number of PCL meshes and tailoring the AMP concentration. Irrevocably, the fiber-reinforced bioactive membrane showed favorable cellular responses, significantly higher rates of mineralization, osteogenic gene expression and *in vivo* bone formation. The enhanced bone formation of the engineered membrane was attributed to the incorporation of the bioactive AMP as well as to the presence of the reinforcing PCL mesh that also reduces the degradability of the membrane *in vivo*. Collectively, membranes based on MEW PCL mesh infused with AMP-laden hydrogel are promising as a cell- and growth factor-free strategy for GBR application. Further studies under a dynamic loading regime *in vitro* and *in vivo* should be performed to fine-tune the intended application in a more clinically relevant GBR scenario.

Acknowledgements

M.C.B. acknowledges the National Institutes of Health (NIH) / National Institute of Dental and Craniofacial Research (NIDCR) (Grants K08DE023552 and R01DE026578). S.B.B. is supported by National Science Foundation (NSF) IR/D program. The content is solely the responsibility of the authors and does not necessarily represent the official views of the National Institutes of Health and the National Science Foundation.

REFERENCES

[1]. Kotela I, Podporska J, Soltysiak E, Konsztowicz K, Blazewicz M, Polymer nanocomposites for bone tissue substitutes, Ceramics International 35(6) (2009) 2475–2480.

[2]. Bodic F, Hamel L, Lerouxel E, Baslé MF, Chappard D, Bone loss and teeth, Joint Bone Spine 72(3) (2005) 215–221. [PubMed: 15850992]

[3]. Bottino MC, Thomas V, Schmidt G, Vohra YK, Chu T-MG, Kowolik MJ, Janowski GM, Recent advances in the development of GTR/GBR membranes for periodontal regeneration—a materials perspective, Dental materials 28(7) (2012) 703–721. [PubMed: 22592164]

[4]. Sheikh Z, Hamdan N, Ikeda Y, Grynpas M, Ganss B, Glogauer M, Natural graft tissues and synthetic biomaterials for periodontal and alveolar bone reconstructive applications: a review, Biomaterials research 21(1) (2017) 9. [PubMed: 28593053]

[5]. Hutmacher DW, Dalton PD, Melt electrospinning, Chemistry–An Asian Journal 6(1) (2011) 44–56.

[6]. Dong L, Wang S-J, Zhao X-R, Zhu Y-F, Yu J-K, 3D-printed poly (ε-caprolactone) scaffold integrated with cell-laden chitosan hydrogels for bone tissue engineering, Scientific reports 7(1) (2017) 13412. [PubMed: 29042614]

[7]. Lee D, Choi EJ, Lee SE, Kang KL, Moon H-J, Kim HJ, Youn YH, Heo DN, Lee SJ, Nah H, Injectable biodegradable gelatin-methacrylate/β-tricalcium phosphate composite for the repair of bone defects, Chemical Engineering Journal 365 (2019) 30–39.

[8]. Kim WJ, Yun H-S, Kim GH, An innovative cell-laden α-TCP/collagen scaffold fabricated using a two-step printing process for potential application in regenerating hard tissues, Scientific reports 7(1) (2017) 3181. [PubMed: 28600538]

[9]. Wang Y, Ma M, Wang J, Zhang W, Lu W, Gao Y, Zhang B, Guo Y, Development of a photo-crosslinking, biodegradable GelMA/PEGDA hydrogel for guided bone regeneration materials, Materials 11(8) (2018) 1345.

[10]. Bas O, D'Angella D, Baldwin JG, Castro NJ, Wunner FM, Saidy NT, Kollmannsberger S, Reali A, Rank E, De-Juan-Pardo EM, An integrated design, material, and fabrication platform for engineering biomechanically and biologically functional soft tissues, ACS applied materials & interfaces 9(35) (2017) 29430–29437. [PubMed: 28816441]

[11]. Castilho M, Hochleitner G, Wilson W, van Rietbergen B, Dalton PD, Groll J, Malda J, Ito K, Mechanical behavior of a soft hydrogel reinforced with three-dimensional printed microfibre scaffolds, Scientific reports 8(1) (2018) 1245. [PubMed: 29352189]

[12]. Visser J, Melchels FP, Jeon JE, Van Bussel EM, Kimpton LS, Byrne HM, Dhert WJ, Dalton PD, Hutmacher DW, Malda J, Reinforcement of hydrogels using three-dimensionally printed microfibres, Nature communications 6 (2015) 6933.

[13]. Zhou H, Nabiyouni M, Lin B, Bhaduri SB, Fabrication of novel poly(lactic acid)/amorphous magnesium phosphate bionanocomposite fibers for tissue engineering applications via electrospinning, Mater Sci Eng C Mater Biol Appl 33(4) (2013) 2302–10. [PubMed: 23498262]

[14]. Klammert U, Ignatius A, Wolfram U, Reuther T, Gbureck U, In vivo degradation of low temperature calcium and magnesium phosphate ceramics in a heterotopic model, Acta biomaterialia 7(9) (2011) 3469–3475. [PubMed: 21658480]

[15]. Babaie E, Lin B, Goel VK, Bhaduri SB, Evaluation of amorphous magnesium phosphate (AMP) based non-exothermic orthopedic cements, Biomedical Materials 11(5) (2016) 055010. [PubMed: 27716636]

[16]. Ribeiro JS, Bordini EA, Ferreira JA, Mei L, Dubey N, Fenno JC, Piva E, Lund RG, Schwendeman A, Bottino MC, Injectable MMP-Responsive Nanotube-Modified Gelatin Hydrogel for Dental Infection Ablation, ACS Applied Materials & Interfaces 12(14) (2020) 16006–16017. [PubMed: 32180395]

[17]. Paul A, Manoharan V, Krafft D, Assmann A, Uquillas JA, Shin SR, Hasan A, Hussain MA, Memic A, Gaharwar AK, Nanoengineered biomimetic hydrogels for guiding human stem cell osteogenesis in three dimensional microenvironments, Journal of Materials Chemistry B 4(20) (2016) 3544–3554. [PubMed: 27525102]

[18]. Carter S-SD, Costa PF, Vaquette C, Ivanovski S, Hutmacher DW, Malda J, Additive biomanufacturing: an advanced approach for periodontal tissue regeneration, Annals of biomedical engineering 45(1) (2017) 12–22. [PubMed: 27473707]

[19]. Nichol JW, Koshy ST, Bae H, Hwang CM, Yamanlar S, Khademhosseini A, Cell-laden microengineered gelatin methacrylate hydrogels, Biomaterials 31(21) (2010) 5536–5544. [PubMed: 20417964]

[20]. Yoshimoto I, Sasaki JI, Tsuboi R, Yamaguchi S, Kitagawa H, Imazato S, Development of layered PLGA membranes for periodontal tissue regeneration, Dent Mater 34(3) (2018) 538–550. [PubMed: 29310906]

[21]. Dalton PD, Vaquette C, Farrugia BL, Dargaville TR, Brown TD, Hutmacher DW, Electrospinning and additive manufacturing: converging technologies, Biomaterials Science 1(2) (2013) 171–185. [PubMed: 32481796]

[22]. Hochleitner G, Chen F, Blum C, Dalton PD, Amsden B, Groll J, Melt electrowriting below the critical translation speed to fabricate crimped elastomer scaffolds with non-linear extension behaviour mimicking that of ligaments and tendons, Acta biomaterialia 72 (2018) 110–120. [PubMed: 29555458]

[23]. Abbasi N, Abdal-hay A, Hamlet S, Graham E, Ivanovski S, Effects of Gradient and Offset Architectures on the Mechanical and Biological Properties of 3-D Melt electrowritten (MEW) scaffolds, ACS Biomaterials Science & Engineering (2019).

[24]. Gupta D, Singh AK, Kar N, Dravid A, Bellare J, Modelling and optimization of NaOH-etched 3-D printed PCL for enhanced cellular attachment and growth with minimal loss of mechanical strength, Materials Science and Engineering: C 98 (2019) 602–611. [PubMed: 30813063]

[25]. Münchow EA, Albuquerque MTP, Zero B, Kamocki K, Piva E, Gregory RL, Bottino MC, Development and characterization of novel ZnO-loaded electrospun membranes for periodontal regeneration, Dental materials 31(9) (2015) 1038–1051. [PubMed: 26116414]

[26]. Thakur T, Xavier JR, Cross L, Jaiswal MK, Mondragon E, Kaunas R, Gaharwar AK, Photocrosslinkable and elastomeric hydrogels for bone regeneration, Journal of biomedical materials research Part A 104(4) (2016) 879–888. [PubMed: 26650507]

[27]. Gaharwar AK, Dammu SA, Canter JM, Wu C-J, Schmidt G, Highly extensible, tough, and elastomeric nanocomposite hydrogels from poly (ethylene glycol) and hydroxyapatite nanoparticles, Biomacromolecules 12(5) (2011) 1641–1650. [PubMed: 21413708]

[28]. Chen X, Bai S, Li B, Liu H, Wu G, Liu S, Zhao Y, Fabrication of gelatin methacrylate/nanohydroxyapatite microgel arrays for periodontal tissue regeneration, International journal of nanomedicine 11 (2016) 4707. [PubMed: 27695327]

[29]. Puppi D, Migone C, Grassi L, Pirosa A, Maisetta G, Batoni G, Chiellini F, Integrated three-dimensional fiber/hydrogel biphasic scaffolds for periodontal bone tissue engineering, Polymer International 65(6) (2016) 631–640.

[30]. Liu J, Li L, Suo H, Yan M, Yin J, Fu J, 3D printing of biomimetic multi-layered GelMA/nHA scaffold for osteochondral defect repair, Materials & Design 171 (2019) 107708.

[31]. Bas O, De-Juan-Pardo EM, Chhaya MP, Wunner FM, Jeon JE, Klein TJ, Hutmacher DW, Enhancing structural integrity of hydrogels by using highly organised melt electrospun fibre constructs, European Polymer Journal 72 (2015) 451–463.

[32]. Bas O, De-Juan-Pardo EM, Meinert C, D'Angella D, Baldwin JG, Bray LJ, Wellard RM, Kollmannsberger S, Rank E, Werner C, Biofabricated soft network composites for cartilage tissue engineering, Biofabrication 9(2) (2017) 025014. [PubMed: 28374682]

[33]. Ren Y, Sikder P, Lin B, Bhaduri SB, Microwave assisted coating of bioactive amorphous magnesium phosphate (AMP) on polyetheretherketone (PEEK), Materials Science and Engineering: C 85 (2018) 107–113. [PubMed: 29407138]

[34]. Dubey N, Ferreira J, Malda J, Bhaduri SB, Bottino MC, Extracellular Matrix/Amorphous Magnesium Phosphate Bioink for 3D Bioprinting of Craniomaxillofacial Bone Tissue, ACS Applied Materials & Interfaces (2020).

[35]. Liu W, Zhan J, Su Y, Wu T, Ramakrishna S, Liao S, Mo X, Injectable hydrogel incorporating with nanoyarn for bone regeneration, Journal of Biomaterials Science, Polymer Edition 25(2) (2014) 168–180. [PubMed: 24138222]

[36]. Nabiyouni M, Ren Y, Bhaduri SB, Magnesium substitution in the structure of orthopedic nanoparticles: A comparison between amorphous magnesium phosphates, calcium magnesium phosphates, and hydroxyapatites, Mater Sci Eng C Mater Biol Appl 52 (2015) 11–7. [PubMed: 25953534]

[37]. Spicer PP, Kretlow JD, Young S, Jansen JA, Kasper FK, Mikos AG, Evaluation of bone regeneration using the rat critical size calvarial defect, Nature protocols 7(10) (2012) 1918. [PubMed: 23018195]

[38]. Bosch C, Melsen B, Vargervik K, Importance of the critical-size bone defect in testing bone-regenerating materials, The Journal of craniofacial surgery 9(4) (1998) 310–316. [PubMed: 9780924]

[39]. Veríssimo DM, Leitão RF, Figueiró SD, Góes JC, Lima V, Silveira CO, Brito GA, Guided bone regeneration produced by new mineralized and reticulated collagen membranes in critical-sized rat calvarial defects, Experimental biology and medicine 240(2) (2015) 175–184. [PubMed: 25245073]

[40]. Kantarci A, Hasturk H, Van Dyke TE, Animal models for periodontal regeneration and peri-implant responses, Periodontology 2000 68(1) (2015) 66–82. [PubMed: 25867980]

[41]. Verna C, Bosch C, Dalstra M, Wikesjö UM, Trombelli L, Healing patterns in calvarial bone defects following guided bone regeneration in rats: A micro-CT scan analysis, Journal of clinical periodontology 29(9) (2002) 865–870. [PubMed: 12423301]

[42]. Gao X, Song J, Zhang Y, Xu X, Zhang S, Ji P, Wei S, Bioinspired design of polycaprolactone composite nanofibers as artificial bone extracellular matrix for bone regeneration application, ACS applied materials & interfaces 8(41) (2016) 27594–27610. [PubMed: 27690143]

[43]. Wang SJ, Jiang D, Zhang ZZ, Chen YR, Yang ZD, Zhang JY, Shi J, Wang X, Yu JK, Biomimetic Nanosilica–Collagen Scaffolds for In Situ Bone Regeneration: Toward a Cell-Free, One-Step Surgery, Advanced Materials 31(49) (2019) 1904341.

[44]. Bubalo M, Lazić Z, Matić S, Tatić Z, Milović R, Petković-Ćurčin A, Đurđević D, Lončarević S, The impact of thickness of resorbable membrane of human origin on the ossification of bone defects: a pathohistologic study, Vojnosanitetski pregled 69(12) (2012) 1076–1083. [PubMed: 23424962]

Statement of Significance

In this study, we developed a fiber-reinforced hydrogel platform with unprecedented tunability in terms of mechanical competence and therapeutic features for guided bone regeneration. We successfully integrated highly porous poly(ε-caprolactone) [PCL] mesh(es) into amorphous magnesium phosphate-laden hydrogels. The stiffness of the engineered hydrogel was significantly enhanced, and this reinforcing effect could be modulated by altering the number of PCL meshes and tailoring the AMP concentration. Furthermore, the fiber-reinforced hydrogel showed favorable cellular responses, significantly higher rates of mineralization, upregulation of osteogenic-related genes and bone formation. In sum, these fiber-reinforced membranes in combination with therapeutic agent(s) embedded in the hydrogel offer a robust, highly tunable platform to amplify bone regeneration not only in periodontal defects, but also in other craniomaxillofacial sites.

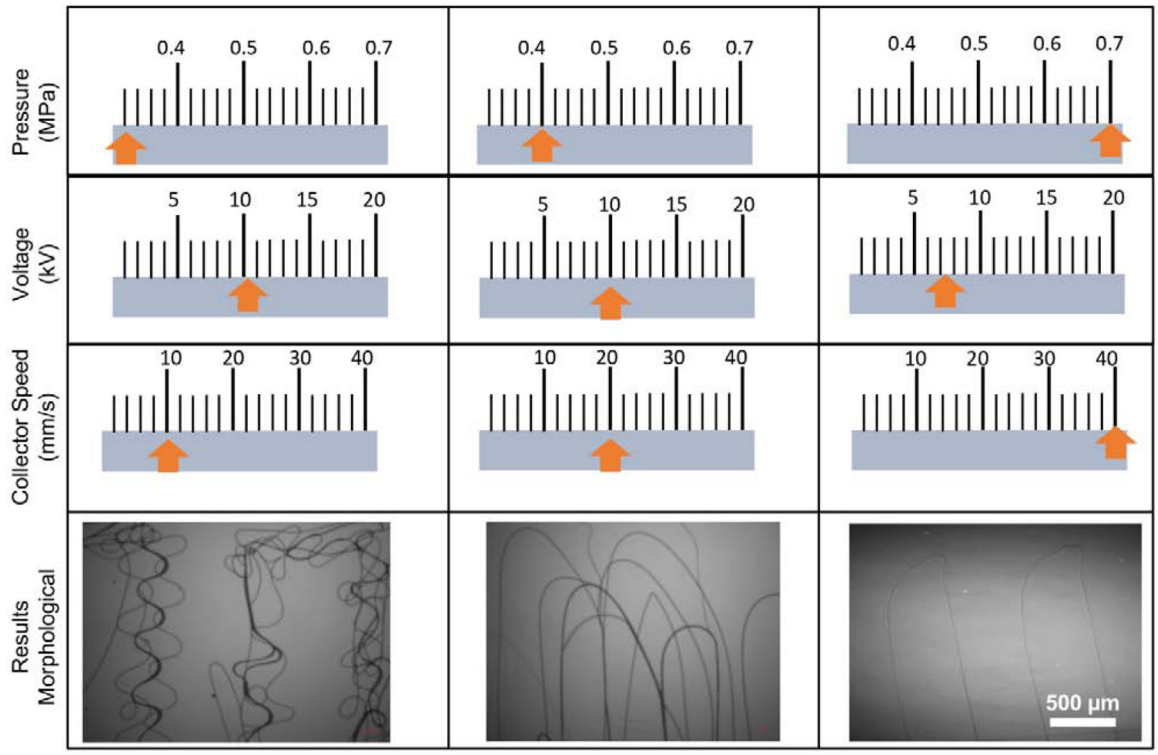

Fig. 1.

Representative values of the processing parameters, namely pressure, voltage and collector speed to reach uniform fibers without buckling. The orange-colored arrows propose values within the respective categories to obtain uniform fibers.

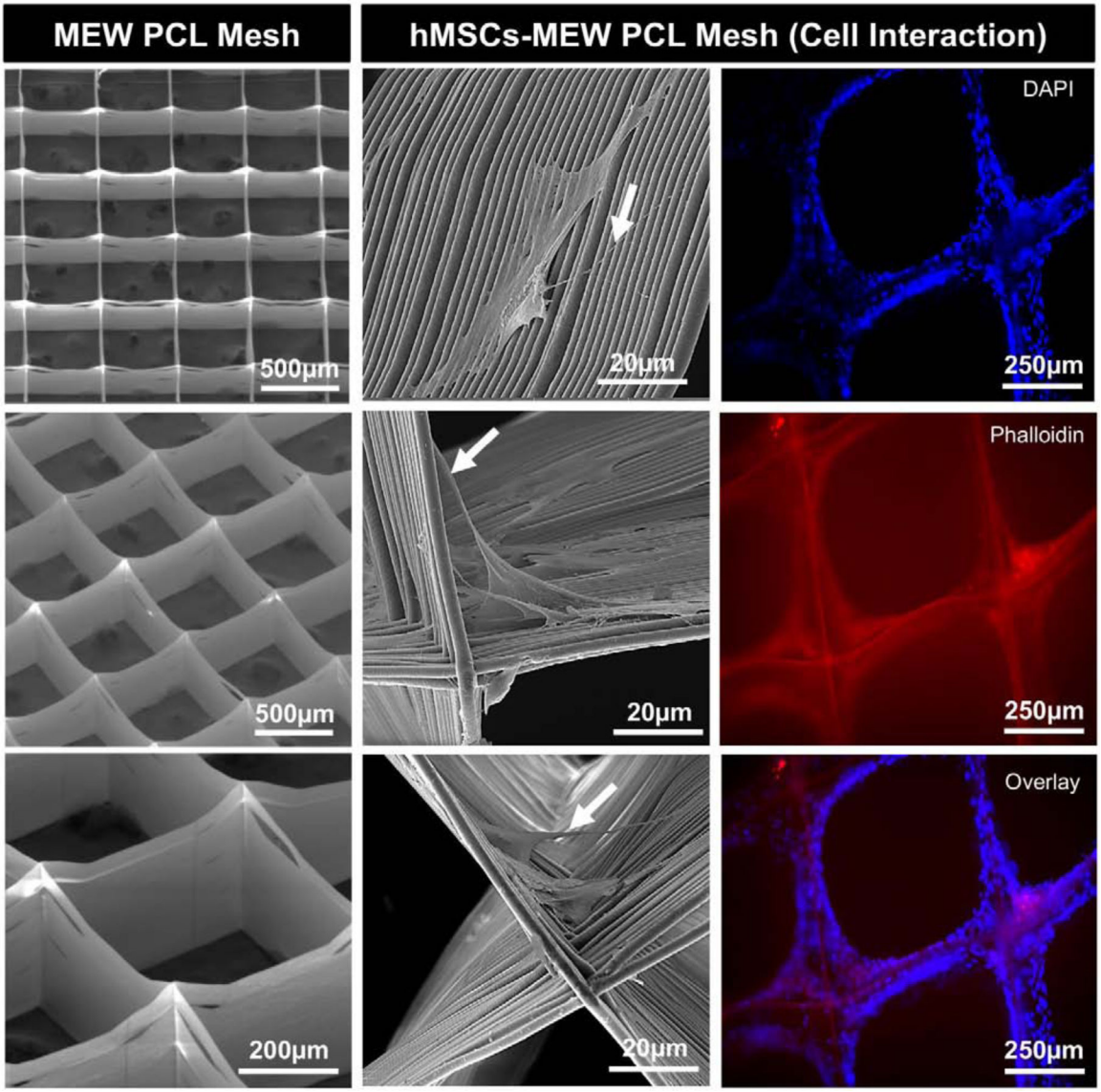

Fig. 2.

(Left) Representative SEM micrographs of MEW PCL mesh show the well-aligned (0–90°-oriented junctions) fibrous 3D architecture with 500 μm pore size and a mean fiber diameter of 3.16 μm. *(Middle)* SEM micrographs of hMSCs-MEW PCL mesh interaction after 3 days of culture. Note significant cell attachment, proliferation, and protrusion along and around the printed PCL fibers. Filopodia are also indicated (white arrows). *(Right)* Fluorescence staining of hMSCs-MEW PCL mesh interaction after 3 days showing phalloidin (Red) staining of filamentous actin and DAPI (Blue) for the nucleus.

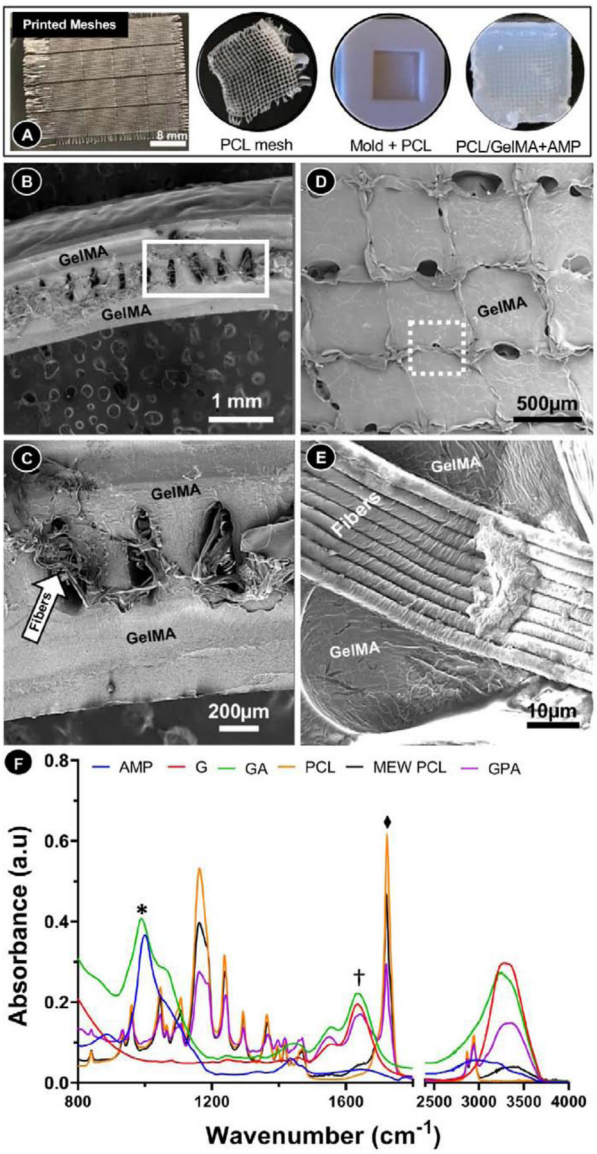

Fig. 3.

(a) Macrophotographs detailing the steps involved in the fabrication of highly porous MEW PCL meshes with well-controlled 3D architecture and infusion with GelMA+AMP using a custom-made mold. (b-e) Representative cross-section SEM micrograph of the GelMA-PCL (GP) membrane showing the hydrogel phase uniformly infiltrated into the pores of the polymer mesh. (f) FTIR spectra showing the functional groups related to phosphate around 1079 cm^{-1} in GelMA+AMP along with typical amide band which is observed in GelMA at 1679 cm^{-1} confirming the incorporation of AMP. (∗, † and ∏ denote AMP-, GelMA- and PCL-related peaks, respectively).

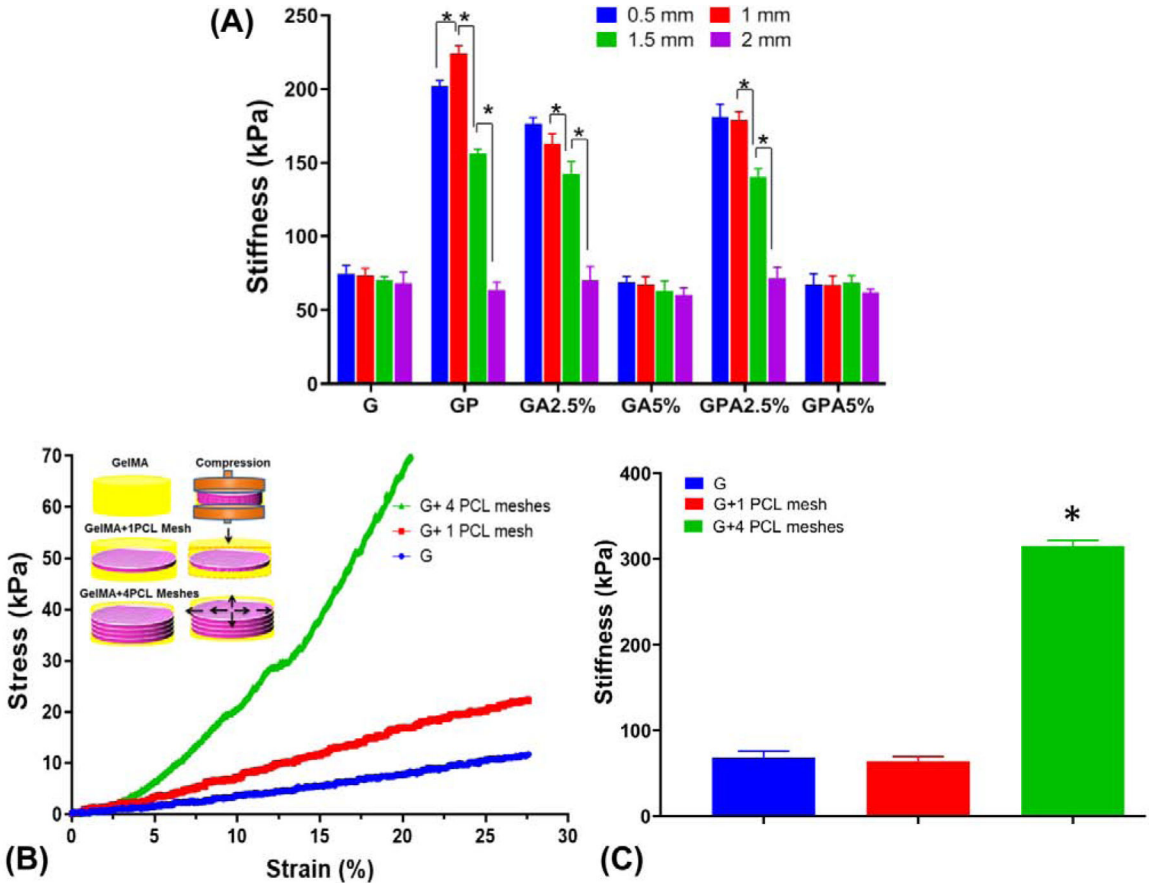

Fig. 4.

(a) Stiffness of GelMA modified with PCL mesh and AMP as a function of hydrogel (membrane) thickness. (b-c) Stress-strain curves and stiffness of GelMA, GelMA with 1 and 4 PCL meshes with schematic showing, when compression is applied to the reinforced hydrogels, the fibers in the hydrogel stretch providing high stiffness and elasticity. (*$p<0.05$).

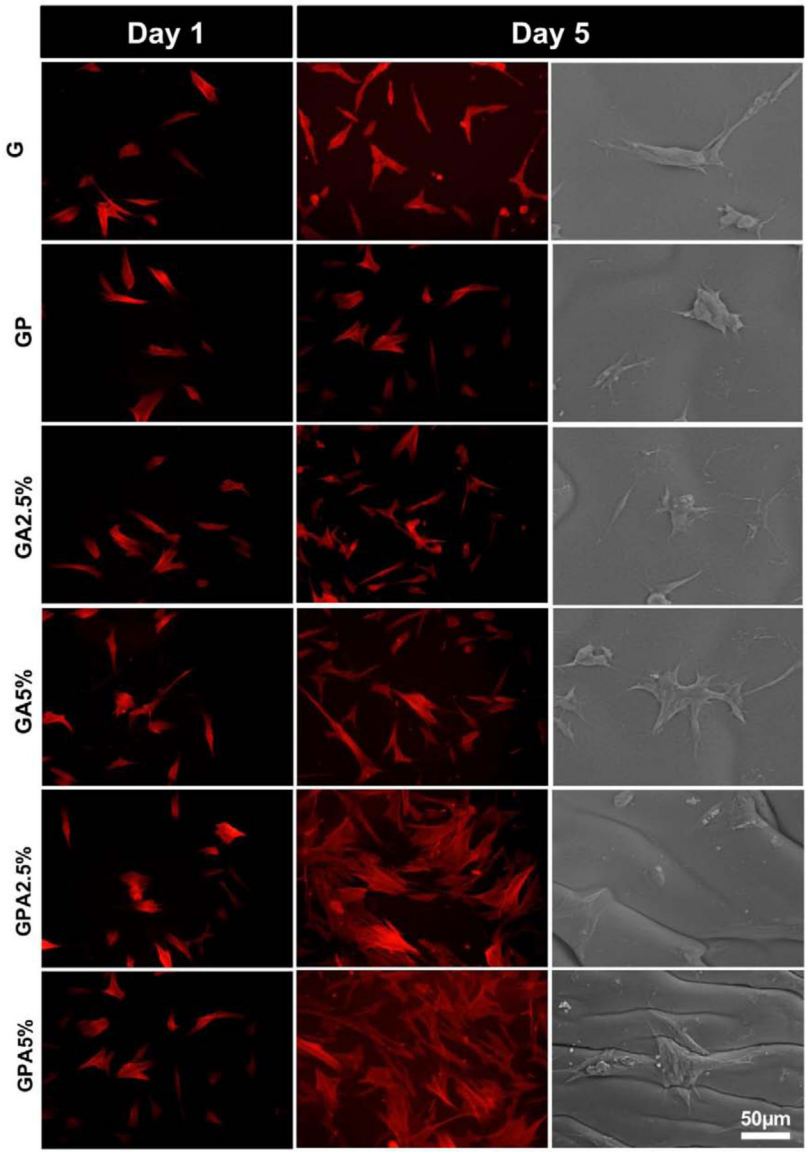

Fig. 5.

Cell attachment, proliferation and spreading. Phalloidin staining showing cells attached and proliferated on developed membrane at day 1 and 5. A significant increase in cell proliferation was noted on GPA membranes (i.e., GPA2.5% and GPA5%) at day 5. SEM micrographs of hMSCs on the various membranes at day 5 showing cell spreading.

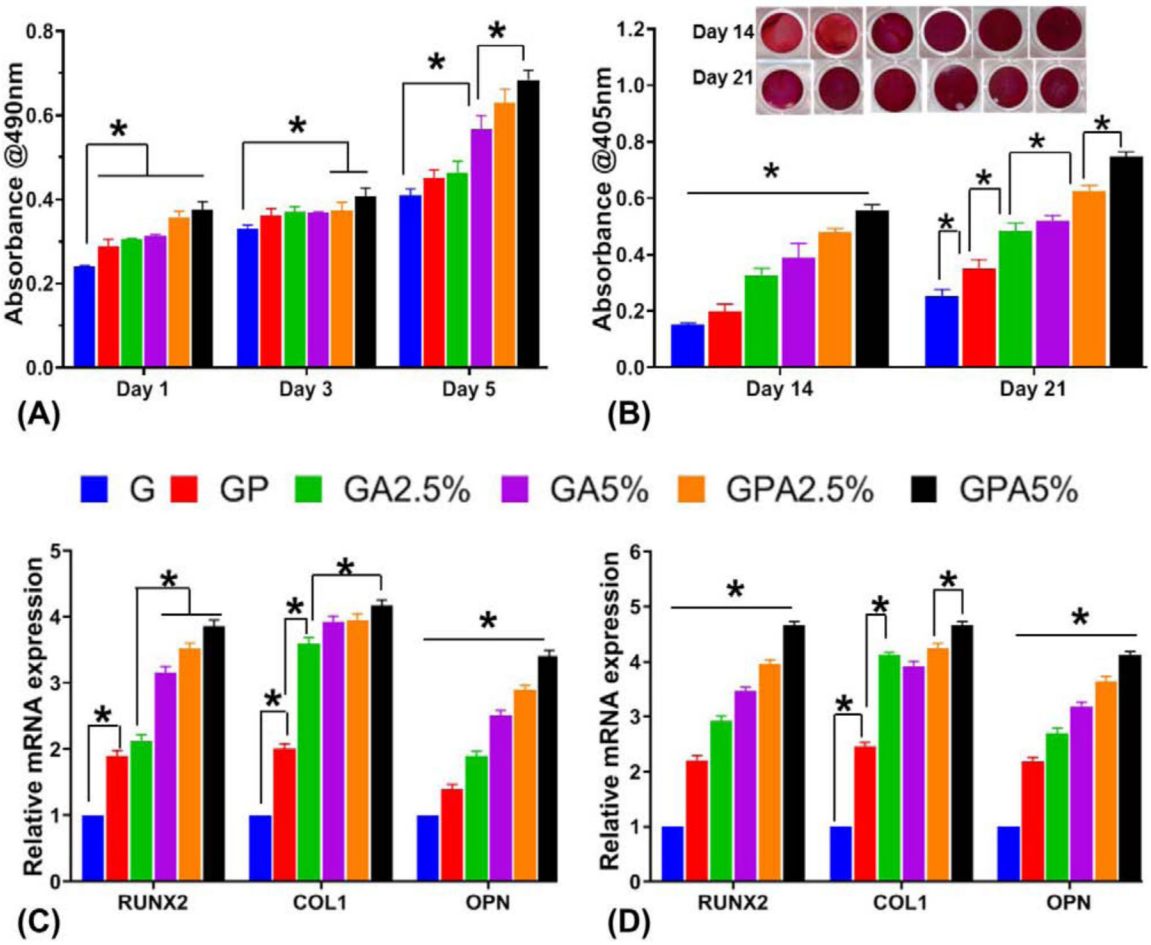

Fig. 6.

(a) Cell viability of hMSCs seeded on the engineered membranes (MTS assay). (b) Qualitative and quantitative assessment of Alizarin red staining showing higher calcium deposits for GelMA+PCL+AMP membranes (GPA2.5% and GPA5%) > GelMA+AMP (GA2.5% and GA5%) > GelMA+PCL (GP) > GelMA (G) after 14 and 21 days. At day 21 there was no significant difference between GA2.5% and GA5%. (C-D) Relative gene expression of bone-related markers of hMSC cultured on the distinct membranes at (c) 14 days and (d) 21 days. All the groups showed significantly higher gene expression in the following order (GPA2.5% and GPA5%) > GelMA+AMP (GA2.5% and GA5%) > GelMA +PCL (GP) > GelMA (G) at all time point. With exception of the expression of Runx2 obtained for GP and GA2.5% for 14 days there was no significant difference (*$p < 0.05$).

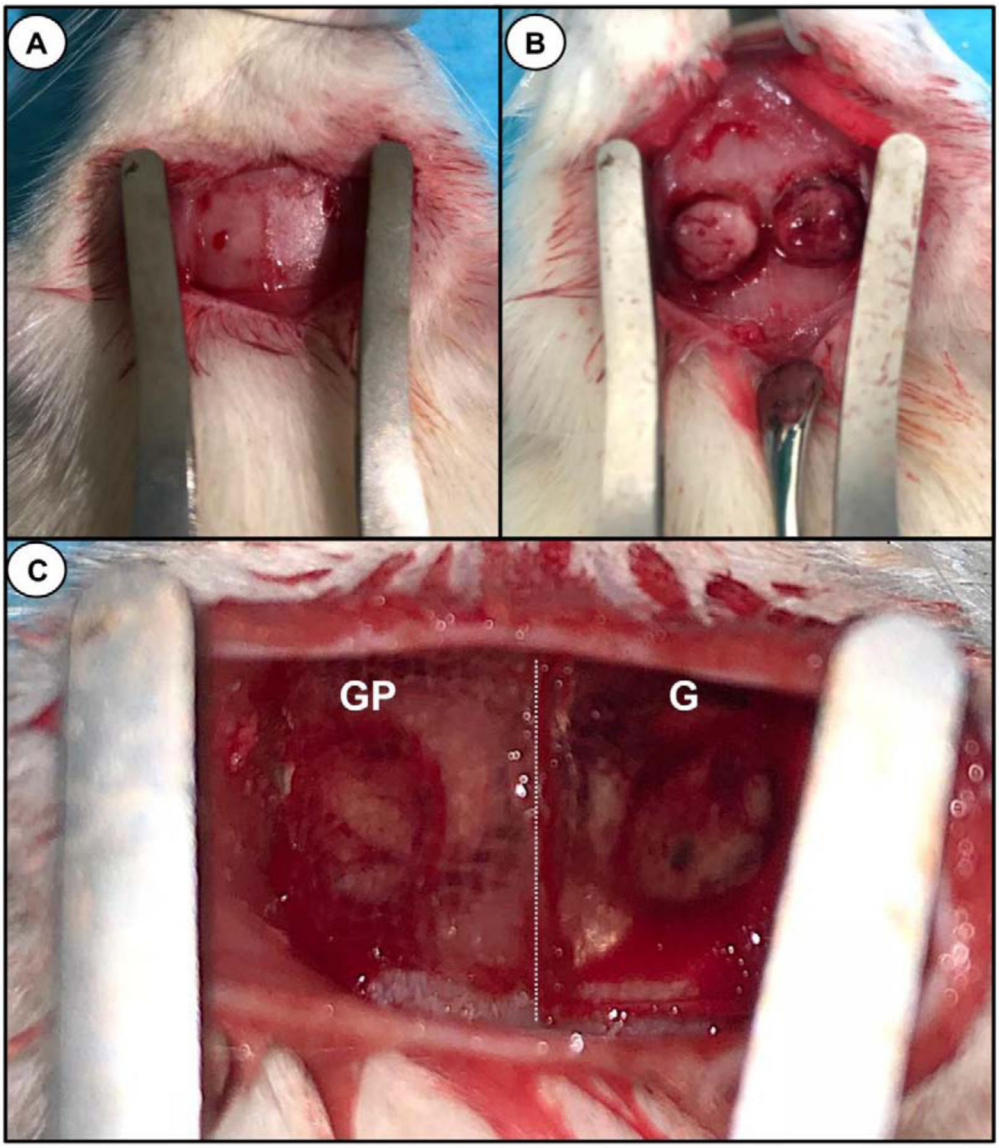

Fig. 7.

Surgical procedures. (a) Rat calvarium exposure (b) Two critical-size bilateral calvaria defects were created using a 5-mm (inner diameter) trephine bur. Care was taken not to injury the dura or superior sagittal vein. (C) Two distinct membranes (8×8 mm^2) were placed over the created bony defects. (Left) Shows a representative macrophotograph of a GelMA-PCL membrane (GP); (Right) GelMA membrane (G). Dotted (white) line demarcating the border between the two surgically placed membranes.

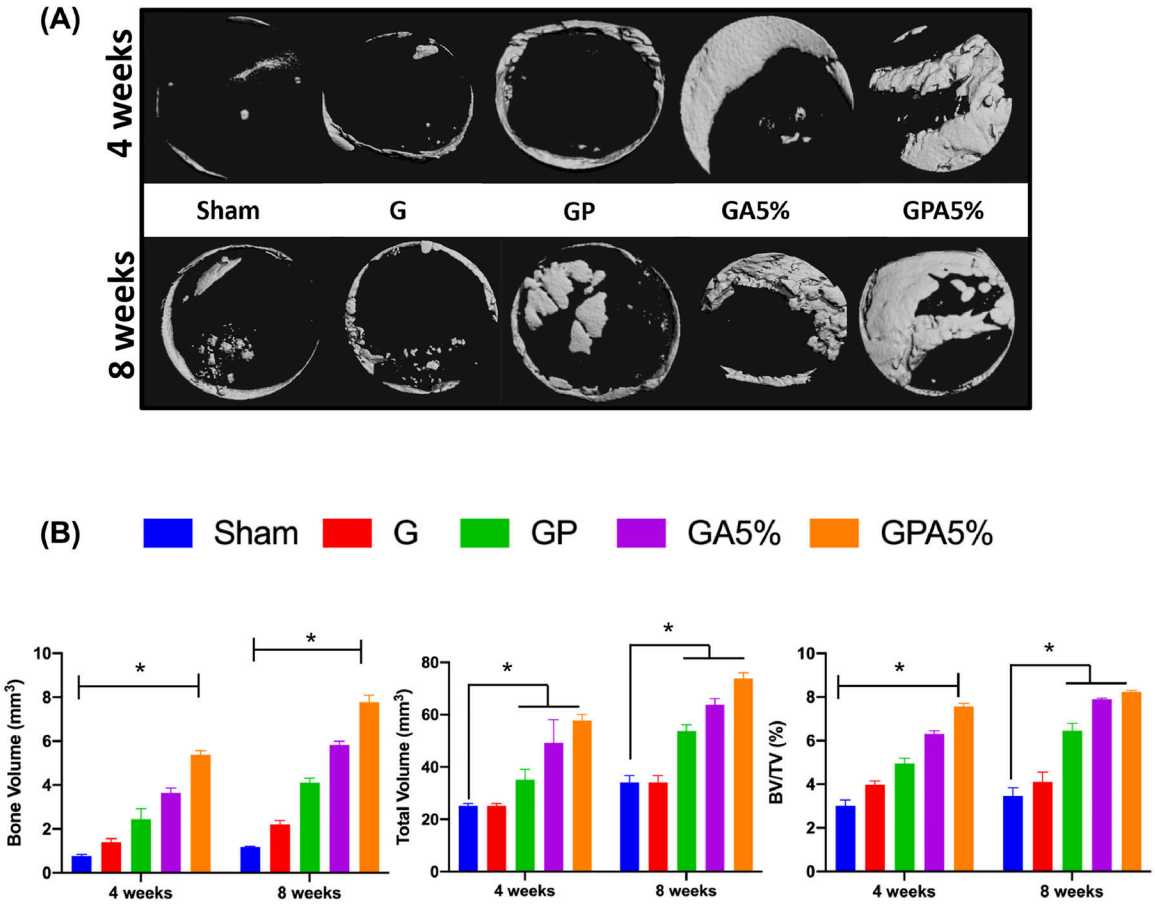

Fig. 8.

(a) Bone defects with or without (sham) membrane were scanned by micro-CT (Scale bar = 1mm). (b) Volume ratios of regenerated bone were quantitatively assessed. At 8-week after implantation, GPA5% had a significantly increased volume ratio of newly formed bone compared with GelMA and Sham. (*$p < 0.05$ compared to Sham – 4 weeks) (mean ± SD, n= 4).

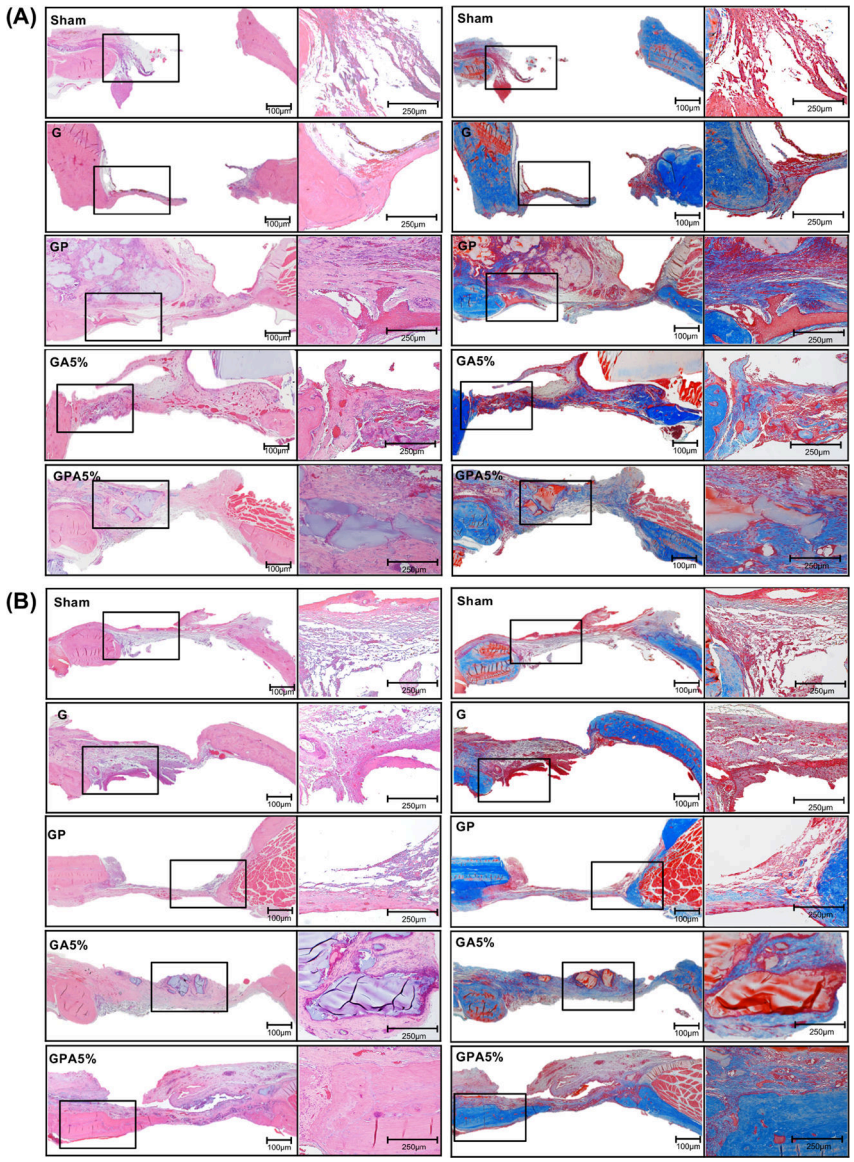

Fig. 9.

Histological view of bone regeneration - (a,b) HE-stained images at 4- and 8-weeks post-implantation, respectively and (C, D) Masson's trichrome-stained at 4 and 8-weeks post-implantation, respectively. The early phase of new bone formation was observed at the margin of the calvarial defect in the positive control and experimental groups. In the negative control, inflammatory cells and collagen fibers were observed. Of note, after 8 weeks, increased bone formation and calcification were observed in all groups, also the clear fusion of new and old bone can be observed at the margin. Magnification x 40 and x100.

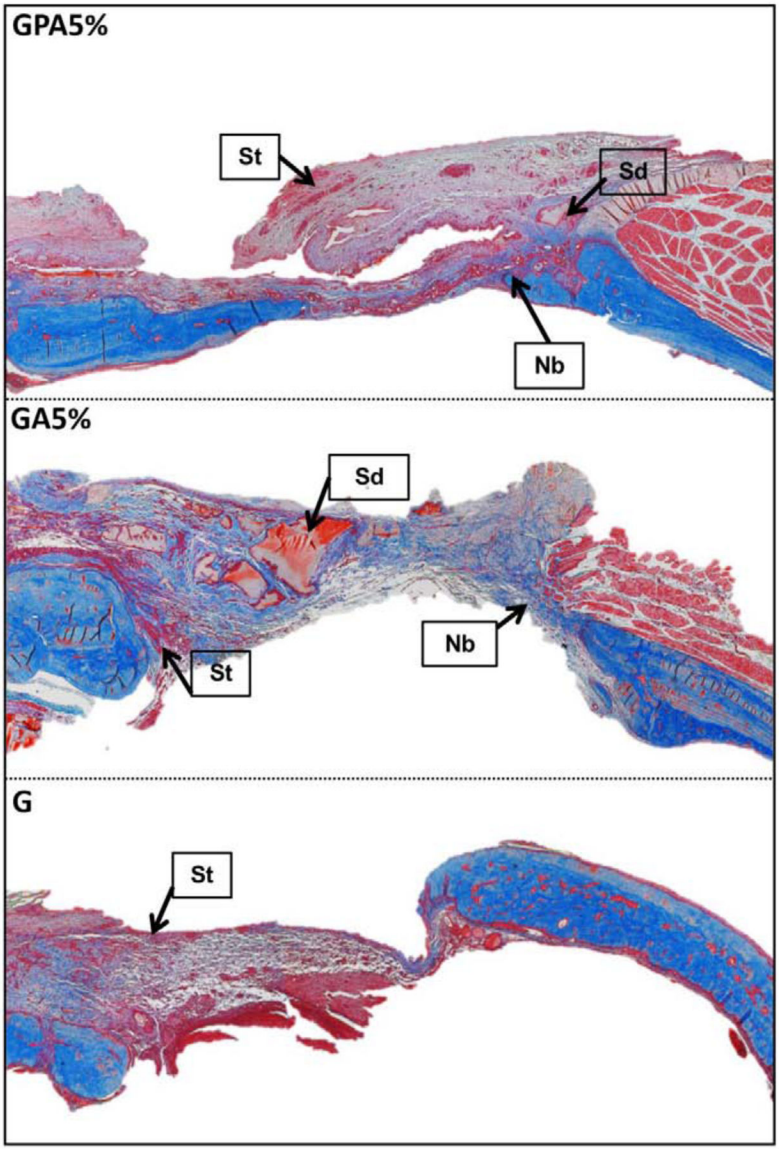

Fig. 10.

Masson's trichrome stained sections of implanted membrane showing the remnants of the GelMA surrounded by newly generating ossifying bone after 8 weeks in the bioactive hydrogel infused in the PCL mesh and bioactive hydrogel group, indicating slower degradation of GelMA in presence of AMP and PCL mesh. In the GelMA alone membrane, the defects were completely filled with loose fibrous tissue without any bone regeneration. St: soft tissue; Sd: GelMA; Nb: new bone.